A Unified System Framework for Hybrid Allocation Optimization and Monte Carlo Reliability Simulation in the Logistics

Simu Zheng *, Ziyi Xu and Yanfeng Li

Xi'an Jiaotong University, Xi'an, China

* Corresponding Author Email: 2256112570@stu.xjtu.edu.cn

Abstract. This paper constructs a unified optimization modeling framework for Earth-Moon cargo transportation and proposes a method that integrates physical mechanism modeling with multi-source transportation coordination and allocation. By establishing a hybrid transportation model that combines elevators and rockets, and introducing an allocation algorithm based on the superposition of throughput capacities, the framework achieves the coordinated optimization of transportation time and cost. Building on this foundation, reliability modeling is incorporated, transforming equipment availability, operational efficiency, and failure probability into a utilization function, while a multi-level stochastic perturbation structure is used to characterize system fluctuations. To analyze the impact of uncertainty, discrete-time Monte Carlo simulation is employed to dynamically evaluate the transport process, enabling the quantitative characterization of delay risks. Concurrently, a capacity margin constraint model is constructed, and key influencing factors are identified using surrogate functions. At the multi-objective level, a coupled model of transportation allocation and emissions is introduced, and environmental impact assessments are conducted through stochastic simulation. Finally, a unified allocation strategy that integrates time, reliability, and environmental constraints is proposed. This strategy offers excellent scalability and general applicability, providing methodological support for resource allocation and risk control in complex transportation systems.

Keywords: Hybrid Allocation Optimization, Multi-objective Optimization, Simulation-driven Decision-making.

1. Introduction

With the growing demand for large-scale space projects, inter-celestial cargo transportation has gradually become a key challenge in complex systems optimization. Such problems typically involve the coordinated operation of multiple transport modes, resource allocation, and the accumulation of uncertainties during long-term operations; their core lies in achieving a dynamic balance between efficiency and cost under multiple constraints. Traditional research has largely relied on modeling single transport modes or static parameter settings, making it difficult to simultaneously capture multi-system coupling relationships and complex environmental disturbances. Particularly in high-intensity operational scenarios, such models exhibit significant shortcomings in adaptability and stability.

Existing methods have primarily focused on optimizing independent subsystems or employing simple linear aggregation strategies, lacking a unified modeling framework to describe the coordination mechanisms among multiple transport channels. Additionally, regarding random disturbances during operation, most approaches rely on post-hoc corrections or empirical parameter adjustments, making it difficult to characterize risk propagation pathways at the model level, thereby limiting the reliability and generalizability of decision outcomes [1].

To address these issues, this paper adopts a holistic systems perspective to construct a unified algorithmic model framework that integrates multiple transport modes. Based on a hybrid transport structure, this framework achieves optimal coordination among different transport channels by introducing a dynamic allocation mechanism. It also embeds reliability-driven stochastic processes within the model, allowing uncertainty to directly influence system evolution. Furthermore, by combining simulation-driven evaluation methods, the framework integrates time, cost, and

environmental impact into a single decision-making system, establishing a unified solution path under multi-objective constraints [2][3].

Using Earth-Moon cargo transportation as a typical application scenario, the method proposed in this paper effectively captures key issues such as multimodal coordination, disturbance propagation, and the amplification of extreme risks, demonstrating strong structural scalability and cross-scenario applicability.

2. Hybrid Allocation Optimization Model for Time–Cost Trade-off in Earth–Moon Logistics

Transporting 10^8 metric tons of construction materials to sustain a lunar colony of 100,000 people introduces a fundamental trade-off between delivery time and system cost. Under ideal operating conditions, three transportation architectures are considered: elevator-only, rocket-only, and a parallel hybrid configuration. The analysis integrates physical modeling, parameter calibration, and allocation optimization to characterize system-level performance across these alternatives.

2.1. Delivery Architecture and System Boundary

The transport system is formulated within a unified Earth–Moon logistics framework, where three candidate architectures are defined.

The elevator-only configuration consists of three Galactic Harbours, each comprising an equatorial Earth Port and two 100,000 km graphene tethers connected to apex anchors. To improve global accessibility, Earth Port locations are determined by optimizing the rotation offset ℓ_0 to minimize the aggregate great-circle distance from ten candidate launch sites. This procedure yields longitudes $-172^\circ, -52^\circ, +68^\circ$. These ports function as dedicated elevator interfaces rather than colocated rocket bases.

Because the system-level throughput specification is inherently ambiguous, multiple interpretations can be constructed. The analysis adopts the parallel-operation configuration as the baseline: $C_E^{\text{sys}} = 3\times 179,000 = 537,000$ t/yr , which reflects simultaneous operation of all three harbors.

The rocket-only configuration relies on a subset of existing launch sites for direct Earth-to-Moon transport. To capture technological heterogeneity, expendable and reusable rockets are modeled jointly through four dimensionless parameters:

$$\alpha = \frac{c_{\text{re}}}{c_{\text{ex}}}, \quad \beta = \frac{\lambda_{\text{re}}}{\lambda_{\text{ex}}}, \quad \gamma = \frac{P_{\text{re}}}{P_{\text{ex}}}, \quad y \in [0,1] \tag{1}$$

where α represents the cost ratio, β the cadence ratio, γ the payload ratio, and y the reusable share. The corresponding relationships are $c_{\text{re}} = \alpha c_{\text{ex}}$, $\lambda_{\text{re}} = \beta\lambda_{\text{ex}}$, $P_{\text{re}} = \gamma P_{\text{ex}}$.

The hybrid configuration operates elevators and rockets in parallel, with the objective of minimizing completion time while determining an optimal mass allocation between the two transport channels.

To ensure consistency along the elevator delivery chain, the apex-to-Moon segment is constrained by

$$Q_{\text{apex}} = \kappa_{\text{apex}} Q_b, \quad \kappa_{\text{apex}} \geq 1 \tag{2}$$

Baseline evaluation yields $C_E^{\text{sys}} / Q_b \approx 0.362$, indicating that $\kappa_{\text{apex}} = 1$ is sufficient to prevent downstream congestion. This implies that throughput limitations arise upstream rather than at the apex launch stage.

2.2. Parameter Calibration

All key parameters are grounded in physical principles or industry-consistent ranges to avoid arbitrary assumptions. To reflect uncertainty, three tiers (optimistic, baseline, pessimistic) are introduced.

The unit cost of elevator transport is decomposed as

$$c_E = c_{\text{elec}} + c_{\text{OM}} + c_{\text{cap}} \tag{3}$$

where the electricity component c_{elec} is derived from the minimum mechanical energy required to lift 1 kg to geostationary orbit while co-rotating with Earth:

$$\Delta e(r) = \mu\left(\frac{1}{R} - \frac{1}{r}\right) + \frac{1}{2}\omega^2\left(r^2 - R^2\right) \tag{4}$$

The corresponding cost is

$$c_{\text{elec}}(r) = \frac{\Delta e(r)}{3.6\times10^6} \cdot \frac{p_{\text{kWh}}}{\eta_E} \tag{5}$$

Under typical ranges $p_{\text{kWh}} \in [0.05, 0.25]$ USD/kWh and $\eta_E \in [0.7, 0.85]$, this yields approximately 0.5–6 USD/kg. Combined with operation, maintenance, and capital costs, representative values of c_E are 0.99, 2.92, and 6.37 USD/kg across the three tiers.

The apex-to-Moon cost factor ρ is defined as the cost ratio between apex-launched and Earth-launched rockets:

$$\rho = f + (1-f)\exp\left(-\frac{\Delta\Delta v}{g_0 I_{\text{sp}}}\right) \tag{6}$$

where $f \in [0.5, 0.8]$ is the fixed-cost share, $I_{\text{sp}} \in [350, 450]$ s is the specific impulse, and $\Delta\Delta v \in [5, 8]$ km/s is the effective velocity saving. The baseline value is set to $\rho = 0.7$.

For the rocket subsystem, expendable payload, launch cadence, and launch cost are set within $P_{\text{ex}} \in [100, 150]$, $\lambda_{\text{ex}} \in [10, 100]$, $c_{\text{ex}} \in [90, 150]$, with baseline reusable parameters $\alpha = 0.8$, $\beta = 1.2$, $\gamma = 0.95$, $y = 0.6$.

2.3. Single-Mode Delivery Models

For the rocket-only configuration, the effective annual throughput is

$$Q_b = 365\lambda_{\text{ex}} P_{\text{ex}}\left[(1-y) + y\beta\gamma\right] \tag{7}$$

The corresponding completion time and year are

$$T_b = \frac{M}{Q_b}, \quad Y_b = 2050 + T_b \tag{8}$$

The unit transport cost is

$$u_b = \frac{c_{\text{ex}}\left[(1-y) + y\beta\alpha\right]}{P_{\text{ex}}\left[(1-y) + y\beta\gamma\right]} \tag{9}$$

leading to total cost: $\text{Cost}_b = Mu_b$.

For the elevator-only configuration, throughput directly limits completion time:

$$T_a = \frac{M}{C_E^{\text{sys}}}, \quad Y_a = 2050 + T_a \tag{10}$$

The total cost includes both elevator transport and the apex-to-Moon segment: $\text{Cost}_a = 10^{11} c_E + \rho M u_b$.

2.4. Hybrid Allocation Optimization

When both subsystems operate in parallel, total throughput is additive. The minimum completion time becomes

$$T_c^* = \frac{M}{C_E^{\text{sys}} + Q_b}, \quad Y_c = 2050 + T_c^* \tag{11}$$

To eliminate idle capacity, the optimal elevator allocation is

$$x^* = \frac{C_E^{\text{sys}}}{C_E^{\text{sys}} + Q_b} \tag{12}$$

The resulting system cost is

$$\text{Cost}_c = x^* \cdot 10^{11} c_E + M u_b \left[1 - x^* (1 - \rho)\right] \tag{13}$$

To support subsequent extensions, the allocation variable is generalized as

$$x_{\text{rec}} = \max\left\{x^*, x_{\text{risk}}, x_{\text{env}}\right\} \tag{14}$$

This formulation provides a direct interface for incorporating reliability and environmental constraints in later sections.

2.5. Results and Baseline Configuration

Under the baseline reuse setting $(\alpha, \beta, \gamma, y) = (0.8, 1.2, 0.95, 0.6)$ and $\rho = 0.7$, the analysis focuses on the parallel-harbor configuration $C_E^{\text{sys}} = 537{,}000$ t/yr, which provides the most practical system interpretation.

Table 1 summarizes completion time, cost, and optimal elevator share across parameter tiers. Several consistent trends emerge. The elevator-only configuration remains cost-efficient but exhibits an impractically long completion horizon. In contrast, the hybrid configuration consistently achieves earlier completion than the rocket-only alternative. Moreover, as rocket performance degrades, the optimal elevator share increases substantially, rising from 8.3% in the optimistic tier to 57.6% in the pessimistic tier.

Under baseline conditions, the rocket-only configuration completes delivery in 2117.4 with a total cost of 86.44 trillion USD, whereas the hybrid configuration advances completion to 2099.5 while reducing cost to 79.62 trillion USD. This demonstrates that partial substitution of rocket transport by elevator capacity can improve both temporal and economic performance.

These results establish the hybrid configuration as the reference operating point. The corresponding allocation x_{rec} is subsequently refined by reliability constraints and environmental limits, forming a unified decision framework.

Table 1. Performance Comparison (Case B)

Tier	P_{ex}	λ_{ex}	c_{ex}	c_E	(b)Rocket-only		(a)Elevator-only		(c) Combo Optimal		
	(t/launch)	(launch/ day)	(MUSD /launch)	(USD/kg)	Y_b	Cost (TUSD)	Y_a	Cost (TUSD)	Y_c	Cost (TUSD)	x^* (%)
Optimistic	150	100	90	0.99	2066.8	54.02	2236.2	37.91	2065.5	52.69	8.3
Baseline	125	30	120	2.92	2117.4	86.44	2236.2	60.80	2099.5	79.62	26.6
Pessimistic	100	10	150	6.37	2302.7	135.06	2236.2	95.18	2157.2	112.09	57.6

3. Reliability-Constrained Stochastic Simulation and Robust System Modeling

Building on the deterministic baseline, the transport system is extended to account for non-perfect operational conditions, including elevator tether disturbances, system downtime, rocket failures, and correlated disruptions. These effects are introduced through a stochastic reliability layer that modifies realized throughput while preserving the underlying system structure.

Rather than treating uncertainty as a post hoc correction, reliability is embedded directly into the transport model. This enables a consistent evaluation of delay risk, identification of dominant uncertainty drivers, and seamless integration of reliability constraints into allocation decisions. The resulting formulation provides the operational bridge between the baseline system (Section 3.1) and the constrained optimization developed in subsequent sections.

3.1. Reliability Modeling Framework

Operational uncertainty is incorporated by scaling nominal throughput with effective utilization factors. The realized annual delivery in year t is given by

$$\dot{M}_E(t) = \eta_E(t)\dot{M}_E^{\text{nom}}, \quad \dot{M}_R(t) = \eta_R(t)\dot{M}_R^{\text{nom}} \tag{15}$$

where $\eta_E(t), \eta_R(t) \in (0,1]$ represent the effective utilization of the elevator and rocket subsystems. The nominal capacities are inherited from the baseline configuration: $M_E^{\text{nom}} = 537{,}000$ t/yr, $M_R^{\text{nom}} = 1.483725 \times 10^6$ t/yr.

To retain physical interpretability, utilization is decomposed into mechanism-level components:

$$\eta_E(t) = A(t)[1-\alpha(t)]S(t), \quad \eta_R(t) = W(t)\pi(t)S(t) \tag{16}$$

where: $A(t)$ captures elevator availability (downtime and repair effects), $\alpha(t)$ represents capacity derating due to tether disturbances, $W(t)$ reflects rocket execution efficiency (scrubs, congestion, repairs), $\pi(t)$ denotes launch success probability, $S(t)$ represents common-mode disruptions affecting both subsystems.

This decomposition allows delay propagation to be traced directly to individual failure mechanisms, rather than treated as an aggregate perturbation.

To maintain consistency with the baseline cost model, unit costs are left unchanged. Reliability effects enter through a failure-induced cost multiplier applied to rocket transport:

$$\text{FailCost}(t) = 1 + \theta[1 - p(t)] \tag{17}$$

where $\theta \approx 0.758$ is calibrated from expected loss severity and mean success probability $\mu_p = 0.995$. This formulation isolates reliability impacts to throughput degradation and failure-induced cost inflation.

3.2. Stochastic Parameterization

Year-to-year variability is represented using parsimonious distributions. Bounded reliability variables follow Beta distributions, while global perturbations are modeled using truncated normal distributions:

$$A(t) \sim \text{Beta}(k_A\mu_A, k_A(1-\mu_A)),\ W(t) \sim \text{Beta}(k_W\mu_W, k_W(1-\mu_W)),\ p(t) \sim \text{Beta}(k_p\mu_p, k_p(1-\mu_p)) \quad (18)$$

To capture nonlinear disruption effects, a multi-layer shock structure is introduced. This includes common-mode shocks, rocket-specific stand-down events, and independent disturbances. The common-mode factor is modeled as

$$S(t) = \begin{cases} s_{\text{shock}} = 0.5, & I_{\text{corr}}(t) = 1 \quad \text{(shock year)}, \\ S_{\text{base}}(t) \sim \text{TruncNormal}(0.90, 0.05; [0,1]), & I_{\text{corr}}(t) = 0 \quad \text{(normal year)}, \end{cases} \quad (19)$$

This layered representation enables the emergence of "risk-cliff" behavior, where small changes in reliability can produce disproportionately large delays.

3.3. Monte Carlo Simulation

System performance under uncertainty is evaluated using a discrete-year Monte Carlo simulation. Two configurations are used: 6,000 runs for convergence and 20,000 runs for accurate tail-risk estimation [4].

The system evolves according to

$$M_{t+1} = M_t + \dot{M}_E(t) + \dot{M}_R(t) \quad (20)$$

with termination condition $M_{2050+T} \geq M$, $Y = 2050 + T$, $\Delta Y = Y - Y^{(Q1)}$.

Setting all stochastic variables to unity recovers the deterministic baseline, confirming model consistency.

The resulting delay distribution is summarized in Table 2, showing a mean delay of 6.38 years and a near-certain probability of multi-year slippage under baseline reliability conditions. The relationship between delay risk and capacity margin is illustrated in Fig. 1, which identifies the minimum margin satisfying $\Pr(\Delta Y_\kappa > 3) \leq 0.05$. The threshold $\kappa = 1.08$ emerges as the minimum requirement for controlling tail risk.

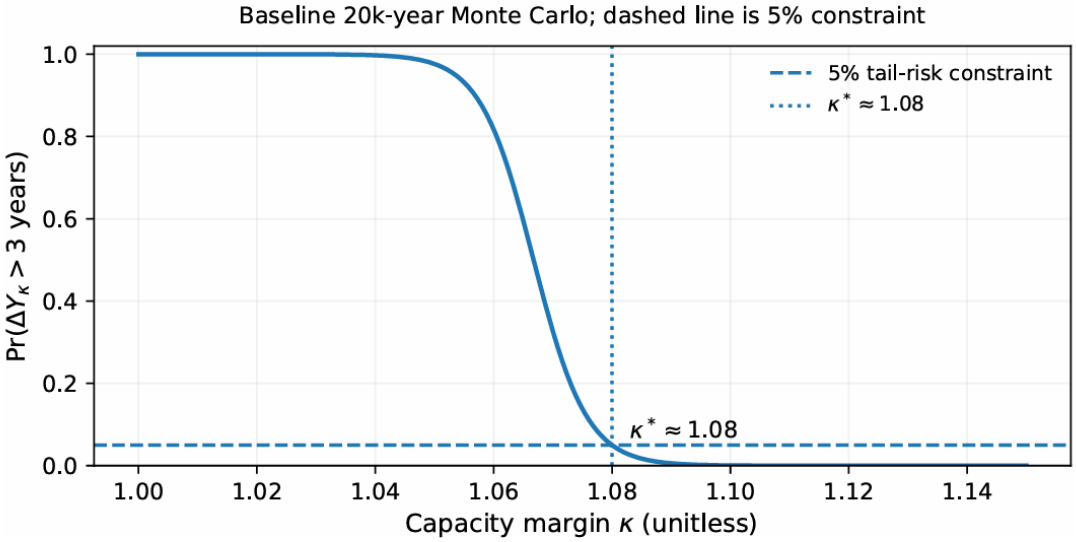

Fig. 1 Tail risk vs. capacity margin κ (20,000 Monte Carlo runs)

Table 2. Baseline Delay Distribution (tail statistics from 20,000 Monte Carlo runs)

Metric	Value
$\mathbb{E}[\Delta Y]$ (yr)	6.38
$\Delta Y_{5/95}$ (yr)	5.64 / 7.18
$\Pr(\Delta Y > 3)$	1.00
$\kappa_{\min}$ (for $\Pr(\Delta Y_{\kappa} > 3) \le 0.05$)	1.08

3.4. Baseline Impact and Key Drivers

Introducing reliability fundamentally shifts system behavior. The expected completion year increases to approximately 2106, compared to 2099.5 under deterministic assumptions. Average utilization levels are $\mathbb{E}[\eta_E] \approx 0.819, \quad \mathbb{E}[\eta_R] \approx 0.910$, while the realized elevator share remains close to the deterministic optimum: $x \approx 0.246$.

This indicates that the hybrid allocation is structurally stable, but highly sensitive to disruption-induced delays.

A surrogate model for mean delay is obtained as $\mathbb{E}[\Delta Y] \approx 1.991 + 14.634(1-\mu_A) + 46.554(1-\mu_W)$, which shows that rocket execution efficiency μ_W dominates delay dynamics, significantly outweighing elevator availability. Reliability therefore affects system performance asymmetrically across subsystems.

3.5. Risk-Constrained Allocation

To incorporate reliability into system design, the minimum elevator share satisfying the schedule-risk constraint is defined as

$$x_{\text{risk}} = \min_{x \in [0,1]} \left\{ \Pr(\Delta Y > 3 \mid x, \mu_A, \mu_W, q_{\text{corr}}) \le 0.05 \right\} \tag{21}$$

Under baseline conditions, no allocation near the deterministic optimum satisfies this constraint. This indicates that feasibility is constrained by reliability rather than nominal capacity.

The dominant mechanism behind delay amplification is orbital-window coupling. Missed launch windows introduce discrete scheduling shifts, which are captured by

$$W(t) = W_{\text{ops}}(t), W_{\text{orb}}(t) \tag{22}$$

$$W_{\text{orb}}(t) = \min\left(1, \frac{N_{\text{win}}(t)}{N_{\text{sched}}(t)}\right) \tag{23}$$

This mechanism explains the emergence of nonlinear delay escalation under high disruption or high-cadence regimes.

Mitigation strategies therefore focus on operational adjustments rather than infrastructure changes. Effective controls include geographic diversification of launch sites, cadence limits at high-latitude locations, preservation of schedule slack, and the introduction of capacity margin κ.

The allocation rule is accordingly updated to

$$x_{\text{rec}} = \max\left\{ x^*, x_{\text{risk}}, x_{\text{env}}, \kappa - \text{adjusted } x \right\} \tag{24}$$

3.6. Summary

Incorporating stochastic reliability fundamentally alters the system's operating regime. Under realistic conditions, multi-year delays become highly probable, and performance is governed by uncertainty propagation rather than nominal throughput.

Rocket execution efficiency emerges as the dominant driver of delay risk, while correlated disruptions introduce nonlinear amplification effects. The capacity margin $\kappa = 1.08$ provides a practical threshold for controlling tail risk.

These results establish the reliability-constrained baseline and directly motivate the environmental feasibility analysis, where reliability and emissions jointly determine the final allocation strategy.

4. Environment-Constrained Optimization Model via Allocation–Emission Coupling

4.1. Core Metrics

Environmental impact is evaluated from the perspective of Earth-side emissions associated with transporting 10^8 t of construction materials. Two complementary indicators are adopted: cumulative carbon emissions E_{CO2} over the full campaign and peak-year stratospheric black carbon injection $B\text{strat}^{\max}$ in Gg/yr. The former captures long-term greenhouse forcing, while the latter reflects extreme atmospheric perturbations linked to stratospheric heating and ozone depletion.

Per-launch emission factors are obtained from Per Launch Emissions.csv, and the mapping from soot loading to climate and ozone response is derived from Stratospheric Response.csv. Taken together, these metrics allow both cumulative and tail environmental effects to be evaluated within a unified framework [5].

4.2. Coupling with Throughput and Reliability

Environmental impact is treated as an endogenous outcome of system design rather than an external constraint. The formulation is therefore directly coupled to the throughput model and the reliability model.

Using the previously defined rocket parameters, the annual transported mass and launch count are

$$\begin{aligned} Q_{\text{rocket}} &= 365\lambda_{\text{ex}} P_{\text{ex}} \left[(1-y) + y\beta\gamma\right] \\ N_{\text{yr}} &= 365\lambda_{\text{ex}} \left[(1-y) + y\beta\right] \end{aligned} \tag{25}$$

The mean payload per launch is $\bar{P} = \dfrac{Q_{\text{rocket}}}{N_{\text{yr}}}$.

For the hybrid architecture, let $x \in [0,1]$ denote the elevator share. The rocket-handled mass is $(1-x)M$, and the corresponding campaign duration is

$$T(x) = \frac{M}{xC_{\text{tot}} + (1-x)Q_{\text{rocket}}} \tag{26}$$

Under the throttled-cadence assumption, annual launches scale proportionally with $(1-x)$, directly linking allocation decisions to emission intensity.

To incorporate disruption effects, correlated outages are modeled through a burst factor

$$B = \frac{1}{1 - q_{\text{corr}}\gamma} \tag{27}$$

which captures the concentration of launches under reduced effective operating windows. The resulting peak-year soot injection is approximated as $B_{\text{strat}}^{\max} \approx B, B_{\text{strat}}$. This formulation highlights a key mechanism: environmental risk depends not only on total launch volume, but also on disruption-induced clustering, which amplifies extreme annual emissions.

4.3. Emission and Response Quantification

Given per-launch emission coefficients e_{CO2} and $e\text{BC}$, cumulative carbon emissions and annual stratospheric black carbon injection are expressed as

$$E_{\text{CO2}}(x) = (1-x)\frac{M}{\overline{P}}, e\text{CO}_2 \tag{28}$$

$$B_{\text{strat}}(x) = \frac{(1-x)N_{\text{yr}}e_{\text{BC}}}{1000} \tag{29}$$

where the factor 1000 converts t/yr to Gg/yr.

Climate and ozone responses are obtained through interpolation on the response dataset, mapping B_{strat} and $B_{\text{strat}}^{\max}$ to ΔT_{sfc} and ΔO_3. This preserves a direct linkage between transport allocation, emission generation, and atmospheric impact.

4.4. Uncertainty Propagation

Environmental performance is evaluated through Monte Carlo simulation, propagating uncertainty in reuse rates, launch performance, payload, emission profiles, and disruption parameters. A total of 80,000 realizations are generated. For each realization, E_{CO2}, $B\text{strat}$, $B_{\text{strat}}^{\max}$, T, ΔT_{sfc}, and ΔO_3 are computed.

The resulting distribution is visualized in Fig. 2, which reveals a clear trade-off structure. The lower-left envelope represents jointly low CO_2 and soot outcomes, while the upper tail reflects disruption-driven amplification of peak emissions. Two patterns emerge. First, increasing elevator share reduces both metrics simultaneously. Second, stratospheric soot exhibits significantly stronger tail sensitivity than cumulative CO_2, indicating that extreme-event risk dominates environmental feasibility.

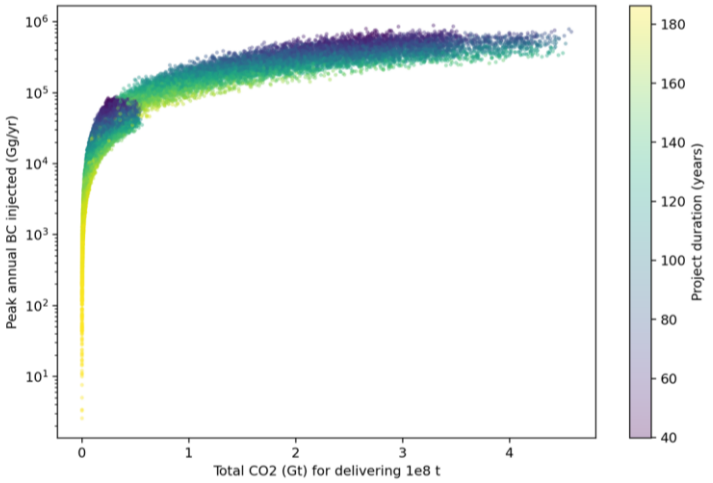

Fig. 2 Monte Carlo trade-off cloud between cumulative CO_2 and peak-year stratospheric soot

4.5. Feasibility Translation and Design Rule

To translate stochastic outcomes into decision constraints, environmental limits are embedded directly into the system-level optimization. For a policy target $\alpha = 0.2$, the environmental threshold

x_{env} is defined as the minimum elevator share satisfying joint caps on CO_2 emissions and peak-year soot.

The feasible region is characterized by Fig. 3, which maps boundary contours in the uncertainty space $(q_{\text{corr}}, \gamma)$. The contour $\Pr\left(B_{\text{strat}}^{\max} > B_{\text{cap}}\right) = 0.05$ defines the safety threshold, while $\Pr\left(B_{\text{strat}}^{\max} > B_{\text{cap}}\right) = 0.5$ marks the onset of a risk-cliff regime. The narrow gap between these contours indicates strong tail sensitivity to correlated disruptions.

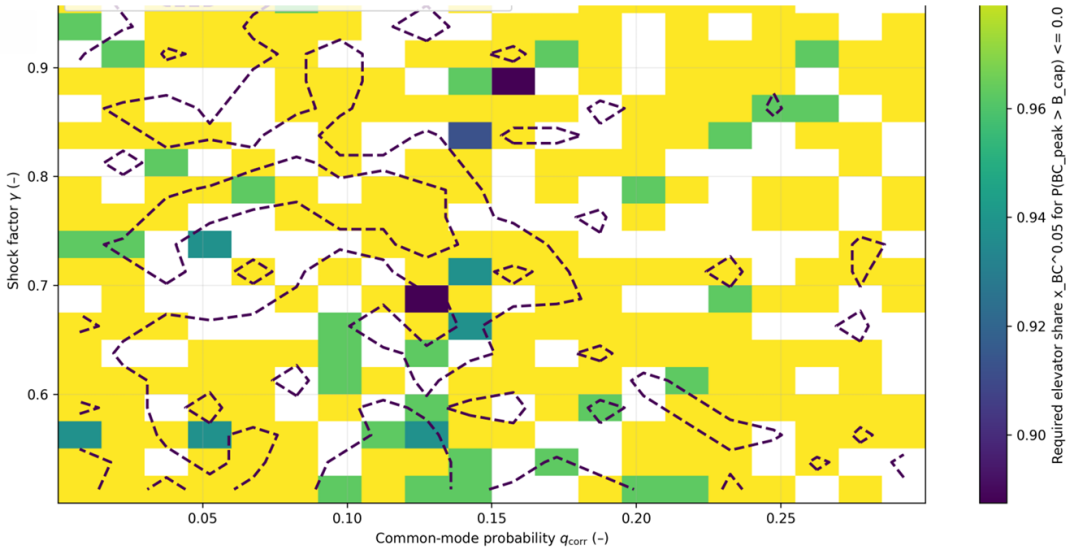

Fig. 3 Environmental feasibility map under correlated disruptions, showing the required elevator share to satisfy peak stratospheric soot constraints

This representation shows that environmental feasibility is fundamentally tail-driven. Correlated outages amplify extreme soot injection far more strongly than they affect average CO_2 emissions. As a result, feasible operation requires remaining within the corridor bounded by the safety threshold while also satisfying cumulative emission constraints.

The resulting multi-objective problem is [6]

$$\min\left(T(x), \text{Cost}(x)\right)$$
$$\text{s.t.} \begin{cases} \Pr\left(\Delta Y > 3 \mid x, \mu_A, \mu_W, q_{\text{corr}}, \gamma\right) \le 0.05, \\ \text{stockout}\left(\tau \mid q_{\text{corr}}, \gamma, L_0, r_{\text{rec}}\right) \le 0.05, \\ PE_{CO_2}(x) \le E_{\max}, B_{\text{strat}}^{\max}(x) \le B_{\max}. \end{cases} \tag{30}$$

Accordingly, the recommended allocation is

$$x_{\text{rec}} = \max\left\{x_{\text{time}}, x_{\text{risk}}, x_{\text{env}}\right\} \tag{31}$$

4.6. Key Outcomes

Environmental feasibility is tightly coupled to both transport structure and disruption dynamics. The Monte Carlo distribution in Fig. 2 quantifies the joint benefit of increasing elevator share, while Fig. 3 translates uncertainty into a feasible operating corridor defined by soot-tail constraints.

These results indicate that environmental acceptability is governed not by average emissions, but by the interaction between launch dependence, correlated disruptions, and extreme annual injection. Under the adopted policy target, the environmental constraint becomes binding, requiring $x_{\text{env}} \gtrsim 0.80$ with even higher values under probabilistic safety requirements.

The final decision variables are summarized in Table 3, where x_{time}, x_{risk}, and x_{env} are integrated into a unified allocation rule. This establishes environmental feasibility as a decisive component of the overall system design.

Table 3. Decision Summary for Final Recommended Elevator Share

Component	Definition	Derivation	Notes	Typical Value
x_{time}	Time-optimal baseline	$x_{\text{time}} = \arg\min_x T(x)$	Case B	≈ 0.27
x_{risk}	Minimum share satisfying reliability constraint	$\Pr(\Delta Y > 3) \le 0.05$	Infeasible under baseline (requires improved μ_A, μ_W, q_{corr})	infeasible
x_{env}	Minimum share satisfying environmental constraints	Emission and resource caps	Evaluated under $\alpha = 0.2$	$\gtrsim 0.80$
x_{rec}	Final recommended share	$x_{\text{rec}} = \max x_{\text{time}}, x_{\text{risk}}, x_{\text{env}}$	Conservative rule	constraint-dependent

5. Conclusion

This paper proposes a unified algorithmic modeling framework for complex transportation systems, enabling the coordinated representation and optimization of multi-modal transportation, stochastic disturbances, and multi-objective constraints. First, by constructing a hybrid model that combines elevator and rocket operations, throughput capacity is coupled with allocation variables to achieve joint optimization of time and cost while ensuring structural consistency. Under the baseline scenario, this approach reduces the completion time from 2117 to approximately 2099 and lowers the overall cost. Second, by introducing reliability-driven utilization modeling and a multi-level stochastic disturbance mechanism, combined with Monte Carlo simulation, we effectively characterize delay distributions and risk amplification effects, revealing that a capacity margin of approximately 1.08 serves as a critical threshold for controlling tail risks. Subsequently, by coupling transportation allocation with emission results, we construct a decision-making model under environmental constraints, enabling the system to achieve a balance between efficiency and emissions. Finally, a unified allocation strategy is formulated, demonstrating good stability and scalability under multi-constraint conditions. Future research could be further extended to more transportation scenarios and dynamic strategy optimization.

References

[1] Luo Rongjuan. Research on Multi-Objective Models and Algorithms for the Loading–Transportation–Distribution Optimization Problem [D]. Northeastern University, 2021. DOI:10.27007/d.cnki.gdbeu.2021.001342.

[2] He Shengxue. Analysis of the Application of Monte Carlo Simulation Techniques in Stochastic Traffic Assignment [J]. 2007.

[3] Zhou Jinlong, Zhang Yinggui, Xiao Yang, et al. Multi-objective Route Optimization Model and Algorithm for Intermodal Transport under Time Uncertainty [J]. Transportation Systems Engineering and Information, 2024, 24(06): 193-205. DOI:10.16097/j.cnki.1009-6744. 2024.06.017.

[4] Chen Chunliang, Qi Ou, Wei Zhaolei, et al. Optimization of Vehicle Equipment Logistics Networks Based on Monte Carlo Simulation and Genetic Algorithms [J]. Journal of Ordnance Engineering, 2016, 37(01): 114-121.

[5] Yang Luojun, Zhang Cheng, Guo Junhua. Research on Multi-Objective Route Optimization for Road-Rail-Water Intermodal Transport under Uncertainty [J]. Journal of East China Jiaotong University, 2023, 40(04): 56-65. DOI:10.16749/j.cnki.jecjtu.2023.04.001.

[6] Yang Jun, Zhan Jun, She Yong. A Multi-Load AGV Scheduling Method for Ports Based on a Multi-Objective Optimization Model [J]. China Navigation, 2022, 45(01): 66-72.